LIMNOLOGY
and
OCEANOGRAPHY: METHODS

Limnol. Oceanogr.: Methods 5, 2007, 317–327

Measuring short-period wind waves in a tidally forced environment with a subsurface pressure gauge

Nicole L. Jones and Stephen G. Monismith*
Environmental Fluid Mechanics Laboratory, Civil and Environmental Engineering, Stanford University, Stanford, CA 94305-4020.

Abstract

The ability of a current meter equipped with a standard pressure sensor to estimate the wave spectra of underdeveloped, fetch-limited waves (peak period ~2 s) in a tidally forced, estuarine environment was investigated. Instruments of this type were placed at four heights throughout the 2.5 m water column, and data were recorded synchronously with a co-located capacitance wave gauge. Linear wave theory was found to adequately describe the wave field in the lower frequency portion of the spectra (<0.6 Hz). The capacitance wave gauge data revealed that the equilibrium range of the spectrum could be modeled as f^{-4}. Large variability in the noise floor of the identical pressure gauges was found. The optimal cutoff frequency (beyond which the f^{-4} model was applied) was defined as the location where the pressure spectra was 12 times the noise floor but was at least 1.1 times the peak frequency. Using these criteria, the pressure sensors measured root-mean-squared wave heights and mean wave periods with an uncertainty of 0.035 m and 0.13 s, respectively (95% confidence level). Applying a point measurement of the current in the transformation of the pressure spectra was found to be as reliable as applying a vertically averaged current. Using the criteria found to best estimate the wave spectra, an expression that determines the ability of a pressure sensor to measure the wave field of interest was developed. This expression enables the user to specify the wind velocity and peak wave frequency at a site and determine the maximum depth below the water surface at which the pressure gauge can be placed.

Short period wind waves (<4 s) can be important to the dynamics of shallow water bodies (<3 m), such as lakes or embayments in estuaries. For example, when waves are long enough to reach the bed, the bed stress is increased, leading to changes in sediment transport (May et al. 2003; Bricker et al. 2005) and, in turn, changes in phytoplankton production (May et al. 2003). Furthermore, the whitecapping of the underdeveloped waves enhances the turbulent kinetic energy in the water column (Terray et al. 1996), influencing vertical mixing of sediment and phytoplankton. In order to characterize the wave conditions in these environments, the use of the subsurface pressure gauges present on modern current meters would be ideal due to their multipurpose abilities and durability. However, the ability of pressure gauges to estimate surface displacement due to underdeveloped, high-frequency waves with relatively small wave heights in a tidally forced environment requires testing.

Subsurface pressure gauges have been used to estimate wave properties for many decades. The popularity of pressure gauges has been maintained due to their low cost, ease of use, and lower susceptibility to damage, given that they are submerged below the water surface. Commercially available current meters commonly have a pressure gauge as part of their standard configuration, allowing directional wave properties to be measured at a relatively low cost and with relative ease of deployment. Unlike surface piercing probes (e.g., capacitance wave gauges), wave-riding buoys, and ultrasonic wave gauges, pressure gauges require assumptions about the transfer function required to convert the pressure signal to a surface elevation signal. Generally this is done by applying linear wave theory (e.g., Smith et al. 2001; Smith 2002; Tsai et al. 2005).

In the presence of currents, linear wave theory is altered due to the Doppler-shift in the wave frequency resulting from the advection of waves by the current. Not including this effect can lead to an underestimation of the wave spectral energy for an opposing current and an overestimation for a

*Present address: School of Environmental Systems Engineering, Mailstop MO15, The University of Western Australia, 35 Stirling Highway, Crawley, WA 6009, Australia; Tel: (+618) 6488-3074

Acknowledgments

Conversations with Ryan Lowe were helpful over the course of this investigation. We would like to thank colleagues from the Environmental Fluid Mechanics Laboratory and the U.S. Geological Survey for their assistance in collecting the data set. The paper also benefited from the comments from two anonymous reviewers. This work was generously supported by the California Bay Delta Authority Restoration Program (ERP02P22) and the Australian Centenary Scholarship program.

following current. This effect becomes significant when the current is similar in magnitude to the phase velocity of the waves and becomes increasingly important in the higher frequency range.

Several authors have studied the effectiveness of applying linear wave theory in the absence of a mean current (Bishop and Donelan 1987; Anctil and Quach 1997; Zaslavskii and Krasitskii 2001; Smith 2002; Lowe et al. 2005; Tsai et al. 2005), as well as in the presence of a current (Gabriel and Hedges 1986; Wolf 1997; Smith 2002). Investigators have also attempted to improve the conversion of subsurface pressure data by considering higher order non-linear terms in the transfer function (e.g., Lee and Wang 1984; Hashimoto et al. 1997). Other investigators have created and tested alternative empirically based transfer functions to transform the pressure signal (Wang et al. 1986; Kuo and Chiu 1994; Tsai et al. 2001). These investigations have shown that linear wave theory adequately transforms the subsurface pressure, and wave heights can be predicted to within approximately 10%, for developed sea and swell conditions. However, the ability of a pressure gauge to estimate surface displacement due to underdeveloped, high-frequency waves with relatively small wave heights in a tidally forced environment has not previously been addressed.

The purpose of this article is to document the performance of a current meter pressure gauge in measuring short period waves in an environment with a sizeable unidirectional velocity and to provide guidelines for achieving the best possible measurements. Measurements with four pressure sensors and a synchronized, collocated surface piercing capacitance wave gauge were used to evaluate the performance of the pressure gauges in a shallow tidal estuary. Issues addressed include the appropriate choice for the current in the pressure data analysis and separating the signal from the inherent noise in the pressure signal at high frequencies. Using the criteria found to optimally estimate the wave spectrum from the pressure gauge data, an expression that determines the ability of a pressure sensor to measure the smallest wave of interest was derived. This expression enables the user to specify the wind velocity and anticipated peak wave frequency at a site to determine the maximum depth below the water surface at which the pressure gauge (with a specified noise floor) can be placed.

Materials and procedures

Analysis of subsurface pressure records—The expression for the subsurface pressure measured by a pressure transducer beneath a progressive wave, assuming linear wave theory and assuming the dynamic pressure is negligible (see "*Noise Considerations*" section) is

$$p = -\rho g z + \rho g \eta K_p \tag{1}$$

where K_p is known as the pressure transfer function

$$K_p(z) = \frac{\cosh k(h+z)}{\cosh kh} \tag{2}$$

Here z is the distance away from the free surface (positive is upward), η is the displacement of the water surface from the mean, k is the wave number, and ω is the angular frequency of the wave (Kinsman 1965).

In the presence of a depth-uniform, unidirectional current, $\bar{u}$, the wave frequency is Doppler-shifted and the dispersion relation becomes

$$\omega_i = \omega_r + \bar{u}(\cos\theta)k \tag{3}$$

where ω_i is the intrinsic radian frequency (i.e., that measured by a stationary wave gauge), θ is the angle between the wave direction and the direction of $\bar{u}$, and ω_r is the frequency relative to a reference frame moving with the component of the current in the wave direction, as given by the dispersion relation

$$\omega_r = \sqrt{gk\tanh(kh)}. \tag{4}$$

To correct for the Doppler shifting effect of the current, Eqs. 3 and 4 are used to solve for the wave number, which is used to calculate the pressure response function via Eq. 2. As $\bar{u}$ approaches the phase velocity of the wave $c = \omega_r / k$, the effect of the current on the transfer function becomes increasingly significant. In general, currents vary with depth, thereby complicating the interaction with waves. The currents within half a wavelength of the water surface have the greatest influence on the waves (Hedges and Lee 1992). Therefore, the optimal estimate for $\bar{u}$ is the equivalent uniform current, U_e, defined by Hedges and Lee (1992) as the uniform current, which produces the same wavelength as the actual depth-varying current for a given wave period, wave height, and water depth. U_e is calculated as the current average from the surface to a depth of $\tanh(kd)/k$. Although, the optimal choice of $\bar{u}$ for use in Eq. 3 is U_e, in the absence of vertical current profiles $\bar{u}$ can be estimated from a point-wise measurement of velocity.

Wind-generated waves are irregular and consist of many frequencies. However, if the displacement of the water surface is assumed to be a zero-mean Gaussian random process, then the surface elevation spectrum, $S_{\eta\eta}(\omega_r)$, can be related to the pressure head spectrum $S_{pp}(\omega_r)$ as follows (Gabriel and Hedges 1986):

$$S_{\eta\eta}(\omega_r) = \frac{1}{K_p^{\,2}} S_{pp}(\omega_r). \tag{5}$$

The spectral forms of the standard wave parameters are then defined with reference to the spectral moments (Wolf 1997)

$$m_n = \int_0^\infty \omega_r^{\,n} S_{\eta\eta}(\omega_r) d\omega_r, \tag{6}$$

such that the root-mean-squared (rms) wave height, H_{rms}, significant wave height, H_s, and mean wave period, $\bar{T}$, are defined as (Wolf 1997)

$$H_{rms} = 2\sqrt{2m_0}, \tag{7}$$

$$H_s = 4\sqrt{m_0}, \tag{8}$$

and

$$\bar{T} = 2\pi\sqrt{\frac{m_0}{m_2}}. \quad (9)$$

Noise considerations—Noise will be present in pressure measurements due to instrumentation factors such as the power system, the pressure transducer itself, the analog filter, and the analog-to-digital conversion (Smith 2002), and environmental factors, such as the accumulation of dirt on the transducer face and flow disturbance around the pressure transducer mount, referred to as hydrodynamic noise (Cavaleri 1980; Bishop and Donelan 1987).

Hydrodynamic noise results from dynamic pressure effects. Dynamic pressures are generated by velocities normal to the sensor face (Kinsman 1965; Cavaleri 1980). For example, when using a Nortek Vector acoustic Doppler velocimeter to profile the water column, Stevens and Smith (2004) found that the pressure data were significantly affected by the dynamic pressure resulting from the water impinging on the pressure sensor face as the instrument ascended at a velocity of 0.15 ms^{-1}. The pressure generated for a velocity, U, is $0.5c_h\rho U^2$, where c_h is a coefficient dependent on the pressure sensor housing (Tucker and Pitt 2001). The largest influence of this term can be removed by orientating the sensor such that the mean flow does not impinge normal to the sensors face. To minimize the smaller components of the dynamic pressure, due to the vertical velocities of the oscillatory and unidirectional flow, as well as any flow disturbances caused by the instrument and mounting frame itself, the pressure sensor should be housed so as to avoid water movement close to the sensor (Cavaleri 1980; Wolf 1997).

Pressure transducers are also sensitive to accumulation of dirt, which can lead to excessive nonlinearity and hysteresis, damping of the high frequency response of the pressure sensor, and possibly a change in the offset relative to the calibration curve (Wolf 1997). These effects can lead to an increase in the wide-band noise floor as well as the possible introduction of systematic errors.

The signal of the pressure spectrum becomes small with respect to the noise floor at high frequencies, while the transfer function, K_p (Eq. 2), approaches zero at high frequencies. Therefore, the transformation of the pressure spectra to the wave spectra via Eq. 5 leads to the noise being amplified in the high frequencies. This can lead to the overestimation of bulk wave parameters such as wave height. Measurement of small, high-frequency waves is particularly sensitive to error of this kind, as the high frequency band of wave energy rapidly attenuates with depth, becoming similar in magnitude to the noise floor of the sensor. There are two techniques commonly employed to prevent the wave spectrum from being contaminated by noise (Smith 2002): (1) subtracting the noise floor from the data before applying the transfer function and (2) truncating the spectrum at a lower frequency than the point where noise begins to dominate. Two techniques are often identified to define this cutoff frequency, f_c: (1) finding the frequency where the transfer function (Eq. 2) is less than 10 to 1000, in which the chosen value depends on pressure sensor resolution (Wolf 1997); and (2) defining the cutoff frequency to occur at the point where the pressure signal is at least an order of magnitude larger than the noise floor, insuring that the pressure signal is not overwhelmed by noise (Smith 2002).

If the wave energy beyond the cutoff frequency is small, this energy can be neglected without introducing significant error in the calculation of the wave parameters. However, when a significant amount of energy exists in the higher frequencies, the wave spectra require extrapolation beyond the cutoff frequency with an appropriately chosen tail, to enable the wave parameters to be adequately estimated. Phillips (1958) proposed that the wave spectrum beyond the peak frequency (i.e., the equilibrium range) should go as ω^{-5}, due to wave breaking limiting the steepness of the wave crests in deep water. Kitaigorodskii (1983) deduced an equilibrium scaling of ω^{-4}, attributable to the non-linear wave-wave interactions that cause an energy cascade. Some empirical evidence has shown this ω^{-4} relationship to be valid (e.g., Miller and Vincent 1990). In practice, investigators have extended the wave spectra by choosing various exponents ranging between –4 and –5 (e.g., Wolf 1997; Smith et al. 2001; Tucker and Pitt 2001; Smith 2002).

Field measurements—Independent measurements of waves were collected in Grizzly Bay, San Francisco Bay, California during May 2005, using four collocated subsurface pressure gauges (0-20 m piezoresistive sensor on Nortek AS, Vector, acoustic Doppler velocimeter [ADV]) at heights of 0.52, 0.86, 1.12, and 1.63 m above the bed and a capacitance wave height gauge (RBR, WG50) (Fig. 1 and Fig. 2). The pressure sensors were oriented such that mean flow did not impinge normal to the sensor faces. The capacitance wave gauge (accuracy 1 cm; precision 1 mm [RBR 2004]) directly measures changes in surface elevation and therefore provides a "true" measurement of the waves for comparison with the transformed data of the pressure gauges. The published accuracy of the Nortek AS ADV 0-20 m piezoresistive pressure sensor is 0.25% of the full scale, and the resolution is stated as being better than 0.005% of the full scale (Nortek-AS 2005).

The instruments were located approximately in the center of the embayment, which has a mean depth of roughly 2.5 m and a mean tidal range of 1.8 m. Depth-averaged maximum currents at the measurement location were approximately –0.15 m s^{-1} on ebb and 0.25 m s^{-1} on flood. For the measurement period, the waves were generally from the southwest to west. The predominant wind direction aligned with the largest fetch, a distance of roughly 13 km, producing relatively large wind waves in Grizzly Bay. The waves present were locally generated with a peak period of approximately 2 s, and significant wave heights ranged between 0 and 0.5 m (Jones and Monismith, 2007). The current usually directly opposed or followed the dominant wave direction for ebb and flood tides respectively.

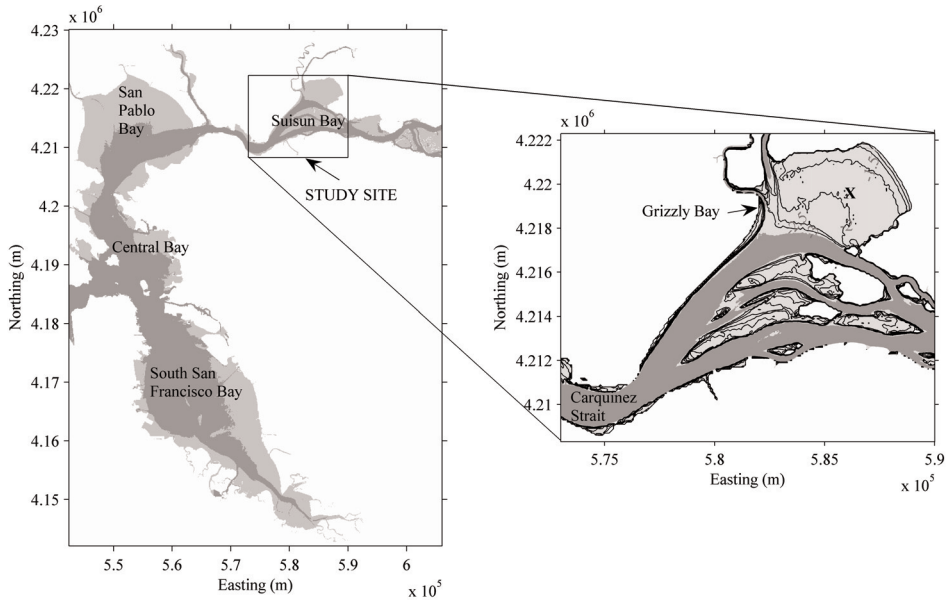

Fig. 1. Bathymetric contours and site map of Suisun Bay showing location of instrument frame (cross). The darker gray areas indicate depth greater than 4 m.

The pressure gauges and capacitance wave gauge were sampled for bursts of duration 10 min at 16 Hz every 30 min for 3 d. Water velocities were measured by the ADVs, and a complete water column mean current profile (10 cm bins) was measured by an acoustic Doppler profiler (Aquadopp Profiler, Nortek AS). The sampling frequency of the pressure data were decreased to 4 Hz by keeping every fourth sample since the time constant of the pressure sensor is 0.1 s (Nortek-AS 2005). The pressure data were corrected for changes in atmospheric pressure so the depth of each pressure sensor was known precisely. Spectral analysis of the pressure and surface elevation signal was achieved by dividing each burst into 16 sections of equal length, each with 50% overlap. Each segment was windowed with a Hanning window and the fast Fourier transform calculated. All 31 spectral estimates were ensemble averaged to produce resultant spectral estimates with 170 degrees of freedom. The expected spectral value is within 0.88 and 1.16 of the sample value at 90% confidence limits (Emery and Thomson 2001).

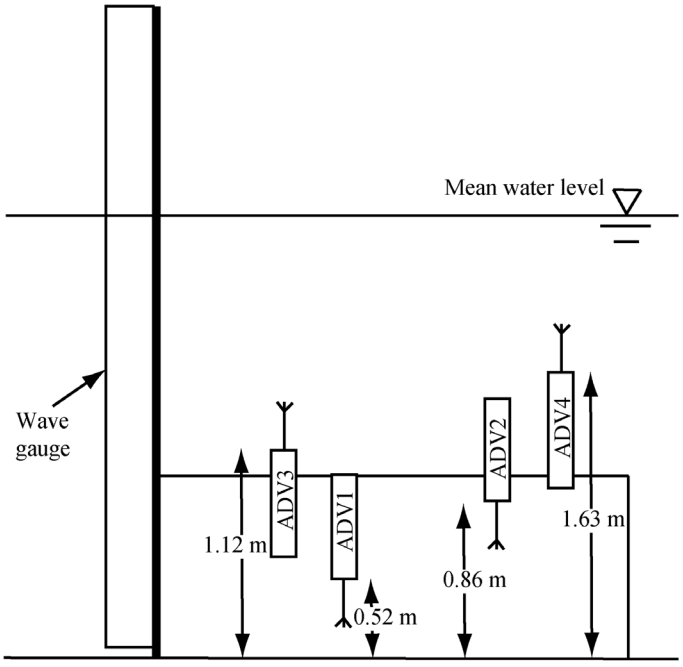

Fig. 2. Schematic of instrument frame. Heights of ADVs indicate location of pressure sensor, relative to the bed.

The equivalent current, U_e, for use in Eq. 3 was determined from 10 min time-averaged data from the acoustic Doppler profiler. The dominant wave direction was estimated via the directional wave spectra using the extended maximum likelihood method (Isobe et al. 1984; Johnson 2002). The Doppler effect of the current was considered negligible for this analysis. The estimate of wave direction was used to calculate the magnitude of the current in the dominant direction of the wave for each burst.

Finally, the appropriate transfer function (Eq. 2) was calculated for each burst. The wave spectrum was then calculated from the pressure spectra using Eq. 5. Wave parameters were then calculated by applying Eqs. 6 to 9.

Assessment and discussion

Figures 3 and 4 are examples of the spectral estimates for a current following and current opposing the wave direction, respectively (calculated as described in "Field Measurements"). Fig. 3A and Fig. 4A contain the spectral density of the raw pressure spectra, S_{pp}, the surface elevation spectra of the capacitance wave gauge, $S_{\eta\eta}$, and the predicted surface elevation

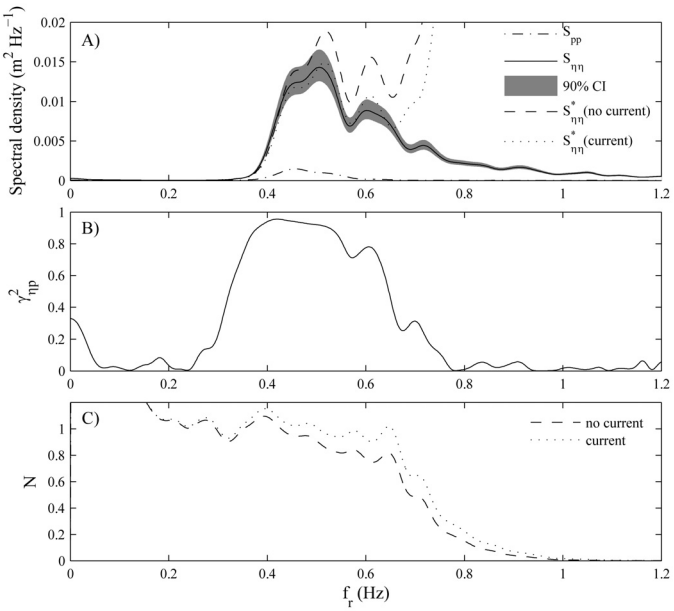

Fig. 3. An example of the spectral properties of ADV2 (0.86 m above the bed) for data collected when the mean current was following the waves, $\bar{u}\cos\theta = 0.1$ m s^{-1}. (A) spectral density, (B) coherence function

spectra, $S^*_{\eta\eta}$, from the transformation of the pressure spectra employing linear wave theory, with and without the inclusion of the Doppler current effect. The transformed spectra, $S^*_{\eta\eta}$, show that disregarding the current led to an overprediction of the wave spectra when the current followed the waves (Fig. 3A) and an under prediction when the current opposed the waves (Fig. 4A). When the Doppler current effect was included in the

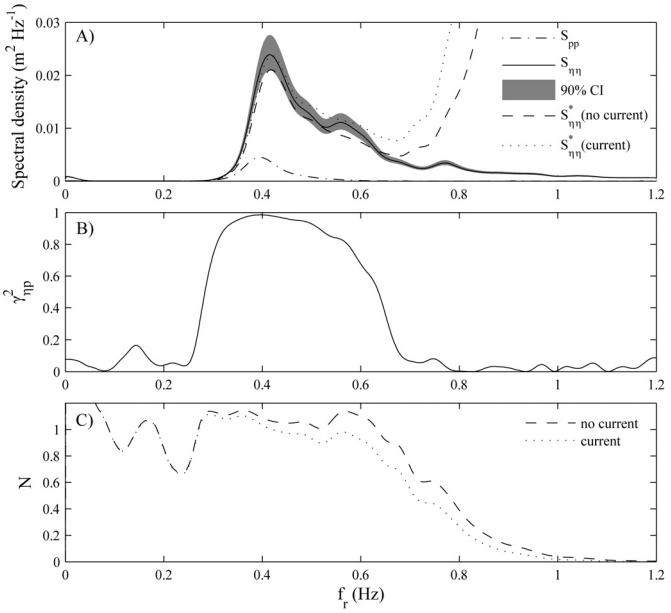

Fig. 4. An example of the spectral properties of ADV2 (0.86 m above the bed) for data collected when the mean current was opposing the waves, $\bar{u}\cos\theta = 0.1$ m s^{-1}. (A) spectral density, (B) coherence function

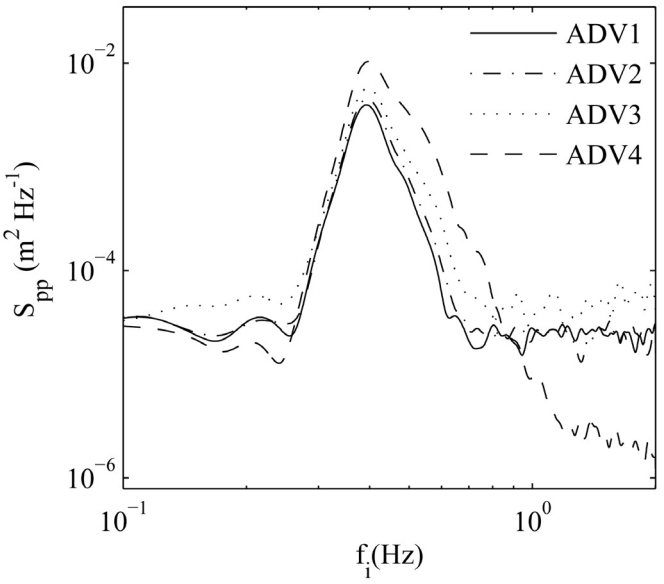

Fig. 5. An example of the raw pressure spectra for the four ADVs. ADV3 has a significantly higher noise floor, at high frequencies, than the other instruments.

pressure data transformation $S^*_{\eta\eta}$ (current) and $S_{\eta\eta}$ agree well for f_r < 0.6 Hz, indicating linear wave theory adequately described the measured wave field. At higher frequencies, $S^*_{\eta\eta}$ (current) deviated from $S_{\eta\eta}$ and monotonically increased. This was due to the transfer function (Eq. 2) approaching zero at high frequencies where the signal-to-noise ratio of the pressure spectra was very low, leading to the amplification of noise in the transformed spectra.

The coherence function is a measure of the correlation between two variables (Bendat and Piersol 2000). The coherence function of the surface elevation measured by the capacitance wave gauge and the subsurface pressure is defined as

$$\gamma_{\eta p}{}^2(\omega) = \frac{|S_{\eta p}(\omega)|^2}{S_{\eta\eta}(\omega)S_{pp}(\omega)}. \qquad (10)$$

in the absence of noise $\gamma_{\eta p}{}^2(\omega) = 1$, and for uncorrelated variables, $\gamma_{\eta p}{}^2(\omega) = 0$. Evidence of the relatively high noise floor of the pressure sensor is shown in the coherence function plots, which fall below 0.9 around a frequency of 0.5 Hz for both the following current (Fig. 3B) and opposing current (Fig. 4B). Comparison with $S_{\eta\eta}$ (Fig. 3A and Fig. 4A) shows that, although this was past the peak frequency, a significant amount of wave energy still existed beyond these frequencies.

Earlier investigators (Gabriel and Hedges 1986; Bishop and Donelan 1987; Kuo and Chiu 1994) introduced an empirical correction factor, *N*, to take into account the differences observed between applying linear wave theory to the subsurface spectral density, S_{pp}, and observed surface elevation spectral density

Table 1. Mean noise floor for the four pressure sensors

	ADV1	ADV2	ADV3	ADV4
Height off bed (m)	0.52	0.86	1.12	1.63
Mean noise floor (m^2/Hz)	2.4×10^{-5}	2.0×10^{-5}	4.0×10^{-5}	2.0×10^{-6}
Single measurement uncertainty R (m)	6.9×10^{-3}	6.3×10^{-3}	8.9×10^{-3}	2.0×10^{-3}

$$N = K_p \left(\frac{S_{\eta\eta}}{S_{pp}} \right)^{1/2}. \quad (11)$$

N was calculated with and without the inclusion of the Doppler current effect (Fig. 3C and Fig. 4C). Over a frequency band of approximately 0.2 to 0.65 Hz, N was close to 1 when the effect of the current was included, indicating that the transfer function, K_p, was adequately described by linear wave theory. At higher frequencies, N decreased toward zero as the pressure signal was attenuated at high frequencies, and the signal became similar in magnitude to the noise floor. In Fig. 3B and Fig. 4B, the coherence function, $\gamma_{\eta p}$, between the pressure and surface elevation was high over the frequency band where N was close to 1 (Fig. 3C and Fig. 4C), in agreement with past results (e.g., Bishop and Donelan 1987).

Inspection of the raw pressure spectra (e.g., Fig. 5) revealed that the four pressure sensors had three distinct wide-band noise floors amongst them, identified by the different energy density values at the highest frequencies (>1 Hz). Here the energy density became constant and the contribution from the noise was larger than the contribution from the signal of interest.

Table 1 displays the average value of S_{pp} in the frequency range of 1.6 to 2 Hz, for each burst, for the entire data set, termed the mean noise floor. Bishop and Donelan (1987) demonstrated that noise in the pressure signal will lead to values of N less than one at higher frequencies. The noise floor for each instrument appeared not to be a function of the depth of the pressure sensor below the free surface, nor a function of the depth-averaged mean water velocity. There was a weak positive correlation between the wave height and magnitude of the noise floor (not shown). This indicated that "hydrodynamic noise" may have contributed to changes in the noise throughout the experiment; however, the data indicated that the largest difference was most likely due to differences in the individual sensors, their related circuitry, and perhaps, the accumulation of dirt in some of the sensors.

The relatively high noise floor of the pressure sensor for ADV3 indicated possible interference with the sensor due to sediment. The pressure sensor on ADV3 was oriented upward; hence sediment was more likely to settle into the sensor housing. However, ADV4 was also oriented upwards and functioned with the lowest wide-band noise floor.

Assuming that the spectral density of the noise had an equal value W in any band, i.e., assuming white or wide-band noise, the single estimate uncertainty R can be estimated from the noise floor W

$$R = \sqrt{\frac{f_s W}{2}}, \quad (12)$$

where f_s is the sampling frequency. The single estimate uncertainty ranged from 2 to 9 mm (Table 1), compared to the 1 mm resolution specified by the manufacturer (Nortek-AS 2005).

Due to the difference in noise floor between the instruments, selecting a cutoff frequency based on the magnitude of the transfer function was not appropriate. Larger errors would have resulted when using ADV3, due to more of the low signal-to-noise portion of the spectrum being included in the wave height calculation. Therefore the cutoff frequency, f_c, was defined as the point past the peak frequency, f_p, where the pressure spectrum, S_{pp}, is a factor of a times greater than the noise floor, W (i.e., $S_{pp}(f_c)/W = a$). A number of values for a were tested to quantify the sensitivity of the estimation of wave parameters to the choice of this number. If the pressure spectrum at the peak frequency was not greater than aW, then the data were unusable. It was further stipulated that f_c had to be greater than a factor of b times the peak frequency, f_p (i.e., $f_c > bf_p$) to ensure f_p was resolved and that the region beyond f_c could be sufficiently well modeled by the equilibrium region theoretical form. Again sensitivity to modification of b was tested.

To enable a deviation from the applicability of linear wave theory to be identified, an average value of N (Eq. 11) was calculated from $N(0.1f_p)$ to $N(f_c)$ for each burst (for $a = 12$ and $b = 1.1$). These values were then averaged for all opposing current bursts and all following current bursts (Table 2). Inadequate numbers of bursts were collected for ADV1 and ADV4 to perform a significant average. This was because the signal-to-noise ratio for ADV1 was often too low, due to its greater depth below the surface and ADV4 was often exposed to air under changing tidal conditions due to its close proximity to the free surface.

Table 2 shows that including the current improved the ability of the linear transfer equation to predict the elevation spectra from the pressure spectra (i.e., N is closer to 1). ADV3 was consistently over-predicting the elevation spectra due to the higher noise floor of this instrument. If the noise is assumed to be wide-band noise (i.e., uniformly distributed over all frequencies), it can be subtracted from the pressure spectrum prior to the transformation (Huntley and Hazen 1988; Trow-

Table 2. Mean values of N for following and opposing currents ($a = 12$ and $b = 1.1$)*

	ADV2	ADV3
Mean N not including current		
Following current	0.9116 (0.0623)	0.8504 (0.0615)
Opposing current	1.0366 (0.0400)	0.9503 (0.0415)
Mean N including current		
Following current	0.9750 (0.0593)	0.8976 (0.0545)
Opposing current	0.9935 (0.0396)	0.9139 (0.0415)

*95% confidence limits for N are shown in parentheses.

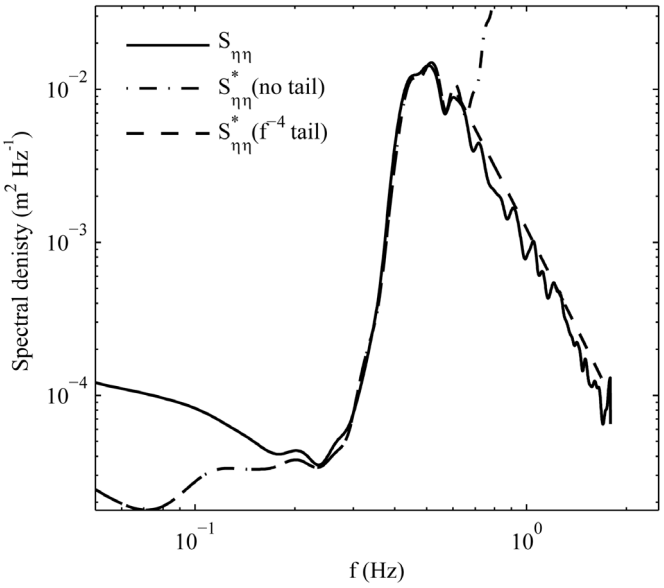

Fig. 6. As shown in this example, the f^{-4} tail generally models the equilibrium range of the wave spectrum successfully.

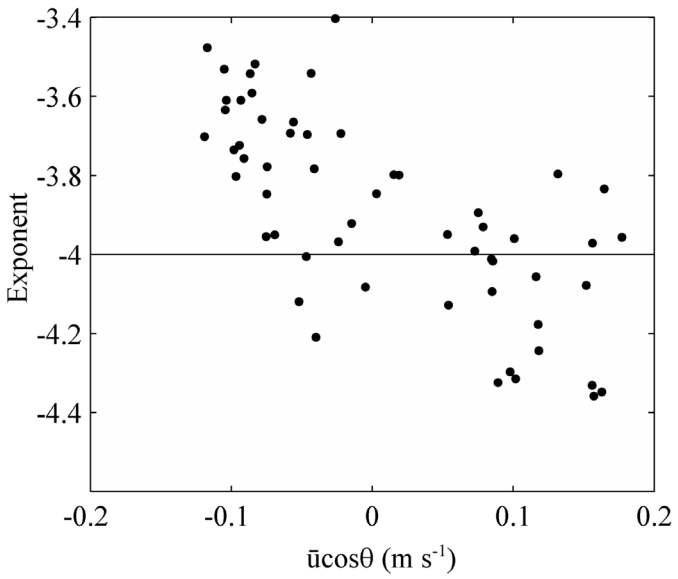

Fig. 7. The exponent describing the decay of the equilibrium range as a function of mean depth-averaged current. When currents oppose the wave direction, the rate of decay of the equilibrium range was found to decrease.

bridge and Elgar 2001). However, following this method led to an underestimation of the estimated elevation spectra (not shown), indicating that the distribution of noise was not uniform over all frequencies.

Significant amounts of wave energy existed beyond the cutoff frequency; therefore modeling the equilibrium range of the wave spectrum was vital to accurately calculate wave parameters. Log-log fits of the equilibrium range of the capacitance wave gauge spectra revealed that the exponent ranged from –4.36 to –3.40 with a mean of –3.89 and a standard deviation of 0.25. Therefore, in general, the application of a f^{-4} tail to the truncated, transformed pressure spectra, $S^*_{\eta\eta}$, matches the capacitance wave gauge data (e.g., Fig. 6). A trend between the current direction relative to wave direction and the exponent was observed (Fig. 7). During periods when currents opposed the waves, the tail decayed less rapidly. However, the differences in the slope of the equilibrium range were not large; therefore the energy of the wave spectra in the high frequencies was modeled effectively with a f^{-4} tail (i.e., beyond f_c), allowing the wave height to be estimated accurately despite the lack of information from the pressure sensors beyond the wave spectrum peak. The f^{-4} tail was appended to the truncated spectrum by specifying this slope to extend beyond $S_{pp}(f_c)$.

A variety of criteria for defining the cutoff frequency were tested in order to ascertain the optimal set of criteria. Table 3 displays the root-mean-square (rms) error in rms wave height, H_{rms}, and mean period, $\overline{T}$, for a selection of test cases. Six test cases are presented: Case 1) Location of the cutoff frequency was where S_{pp} was 12 times the noise floor but was at least $1.1f_p$ (a = 12 and b = 1.1). The effect of the current was neglected in this case; Case 2) identical to Case 1 with the exception that the effect of the current was included; Case 3) location of the cutoff frequency was where S_{pp} was 30 times the noise floor but was at least $1.1f_p$ (a = 30 and b = 1.1); Case 4) Location of the cutoff frequency was where S_{pp} was 12 times the noise floor but was at least $1.2f_p$ (a = 12 and b = 1.2); Case 5) location of the cutoff frequency was where S_{pp} was 5 times the noise floor but was at least $1.1f_p$ (a = 5 and b = 1.1); Case 6) identical to case 1 with the exception that the effect of the current was included. Here $\overline{u}$ was approximated by the corresponding local burst averaged ADV velocity. The more stringent the criterion, the smaller the number of bursts for which wave parameters were calculated. Therefore this number was included in the table.

The first error values presented in Table 3 are for the case where the influence of the current was ignored (Case 1). Overall the error in wave height and mean period was significantly (95% confidence level) decreased when the Doppler effect due to the current was included and the definition of the cutoff frequency remained the same (Case 2, "all" column). However, the error in H_{rms} for ADV1 increased when the Doppler effect of the current was included, although the error in the mean period significantly decreased.

For Cases 3 and 4, more stringent criteria were applied to attempt to further reduce the error in H_{rms} and $\overline{T}$. This resulted in large decreases in the number of bursts analyzed, however, no significant difference in the error was achieved. Case 5 defined the location of the cutoff frequency as where S_{pp} was 5 times the noise floor but was at least $1.1f_p$. These less stringent criteria led to significantly larger rms errors in the wave height and wave period estimation. Therefore, the criteria used in Case 2 were selected as optimal.

As discussed in *Materials and procedures*, the optimal choice of $\overline{u}$ for use in Eq. 3 is the equivalent uniform current U_e, however, in the absence of vertical current profiles $\overline{u}$ can be esti-

Table 3. rms error in rms wave height and mean period estimates at 95% confidence level for six test cases with different definitions of the cutoff frequency*

Case	Description		all	ADV1	ADV2	ADV3	ADV4
1	$12W^{\dagger}1.1f_p$ no current	rms error in H_{rms} (m)	0.046	0.034	0.051	0.053	0.041
	($a = 12$, $b = 1.1$)		(0.042,0.052)	(0.028, 0.034)	(0.043, 0.063)	(0.044, 0.067)	(0.032, 0.056)
		rms error in (s)	0.28	0.25	0.30	0.30	0.33
			(0.25, 0.28)	(0.21, 0.32)	(0.25, 0.37)	(0.25, 0.38)	(0.26, 0.45)
		Nr of bursts analyzed	170	45	54	43	28
2	$12W1.1f_p$	rms error in H_{rms} (m)	0.035	0.044	0.027	0.041	0.026
	($a = 12$, $b = 1.1$)		(0.032, 0.039)	(0.036, 0.056)	(0.023, 0.033)	(0.034, 0.052)	(0.021, 0.035)
		rms error in $\overline{T}$(s)	0.13	0.15	0.11	0.13	0.17
			(0.12, 0.15)	(0.12, 0.19)	(0.09, 0.14)	(0.11, 0.16)	(0.13, 0.23)
		Nr of bursts analyzed	170	45	54	43	28
3	$30W1.1f_p$	rms error in H_{rms} (m)	0.034	0.044	0.029	0.040	0.024
	($a = 30$, $b = 1.1$)		(0.030, 0.039)	(0.035, 0.060)	(0.024, 0.037)	(0.032, 0.054)	(0.019, 0.033)
		rms error in $\overline{T}$(s)	0.13	0.16	0.12	0.15	0.11
			(0.12, 0.15)	(0.13, 0.22)	(0.10,0.15)	(0.12, 0.20)	(0.09, 0.15)
		Nr of bursts analyzed	128	29	40	31	28
4	$12W1.2f_p$	rms error in H_{rms} (m)	0.031	0.038	0.022	0.037	0.025
	($a = 12$, $b = 1.2$)		(0.028, 0.035)	(0.031, 0.050)	(0.018, 0.028)	(0.030, 0.049)	(0.021, 0.035)
		rms error in $\overline{T}$(s)	0.13	0.14	0.10	0.14	0.17 (0.13, 0.23)
			(0.12, 0.15)	(0.11, 0.19)	(0.08, 0.13)	(0.11, 0.18)	
		Nr of bursts analyzed	134	33	40	34	27
5	$5W1.1f_p$	rms error in H_{rms} (m)	0.046	0.053	0.033	0.054	0.050
	($a = 5$, $b = 1.1$)		(0.042, 0.051)	(0.045, 0.066)	(0.028, 0.040)	(0.045, 0.068)	(0.040, 0.068)
		rms error in $\overline{T}$(s)	0.25	0.21	0.20	0.45	0.17
			(0.23, 0.28)	(0.18, 0.26)	(0.17,0.24)	(0.38, 0.56)	(0.13, 0.23)
		Nr of bursts analyzed	194	54	63	49	28
6	$12W1.1f_p$ Local	rms error in H_{rms} (m)	0.036	0.044	0.026	0.044	0.026
	ADV current		(0.032, 0.040)	(0.036, 0.056)	(0.022, 0.032)	(0.036, 0.057)	(0.021, 0.035)
	($a = 12$, $b = 1.1$)	rms error in $\overline{T}$(s)	0.16	0.16	0.15	0.17	0.19
			(0.14, 0.18)	(0.13, 0.20)	(0.13, 0.19)	(0.14, 0.22)	(0.15, 0.26)
		Nr of bursts analyzed	157	42	49	39	27

*A full description of the six cases is given in the text. The 95% confidence intervals for each rms error estimate are given in brackets.
†W is the noise floor; f_p is the peak frequency; nr. of bursts analyzed is the number of bursts that passed the criteria for analysis.

mated from the local ADV velocity (Case 6). The local velocity measured by ADV1 and ADV2 was on average within 0.03 m s^{-1} of U_e and that measured by ADV3 was within 0.04 m s^{-1} on average. Accordingly, there was no significant difference in error for H_{rms} or $\overline{T}$ between Case 2 and Case 6. There was a larger average difference between the point-wise velocity measured by ADV4 and U_e of 0.07 m s^{-1}, however there was still no significant difference in the error for H_{rms} or $\overline{T}$. A current sampled closer to the bed or in a less-developed flow may appreciably underestimate U_e therefore leading to larger errors in the estimation of wave heights and periods (e.g., Smith 2002).

Figure 8 shows a comparison of H_{rms} measured by the capacitance wave gauge with H_{rms} determined by the pressure gauges using the Case 2 criterion. In general there were small errors in the estimation of the wave height. However, for rms wave heights greater than approximately 0.2 m, the wave height estimated by the four pressure gauges displays a tendency to be overestimated (Fig. 8). This is likely due to the dynamics of wave growth at the site. Wave growth was depth limited when the water was shallowest and the pressure gauges were closer to the water surface. As the water depth increased, the waves could grow to larger heights, however the ability of the pressure gauge to respond to higher frequency components was reduced. This resulted in the peak frequency being close to the point where the signal was likely to be overwhelmed by noise, resulting in a greater chance of noise being amplified during the transformation of the pressure spectra, and thereby an overestimation of wave height. These bursts can be removed from the analysis by applying a more stringent rejection criterion; however, although a bias is present the error is small. Figure 8 shows that H_{rms} estimated for ADV1 strongly displayed this bias. All estimates of $H_{rms} > 0.2$ m for ADV1 were under following current conditions, therefore neglecting the Doppler-shift effect of the current resulted in a reduced error in the estimation of H_{rms} (Table 3). However,

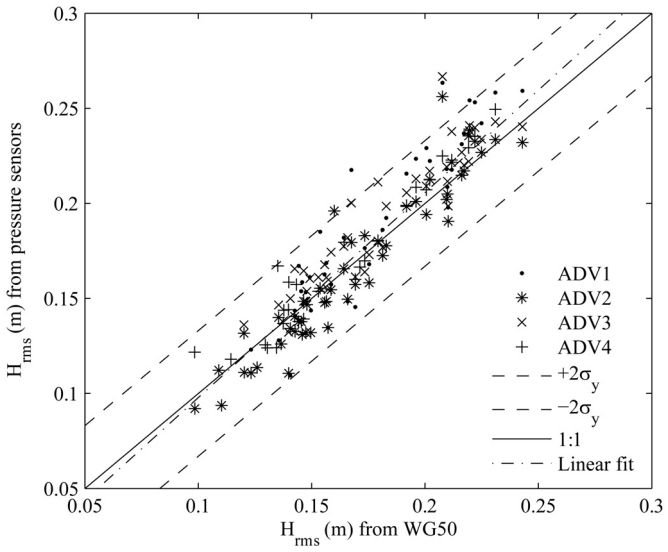

Fig. 8. Comparison of rms wave height estimates (Case 2) from the pressure gauges with the capacitance gauge measurements. The solid line shows the 1:1 relationship, and the dashed lines are the error in the measurements at a 95% confidence level.

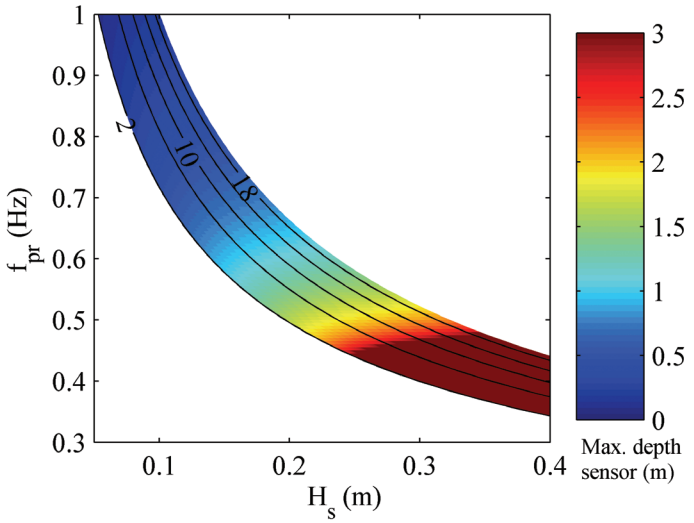

Fig. 9. Maximum depth of immersion of pressure sensor to enable measurement of wave, as a function of significant wave height H_s and peak relative frequency f_{pr} and wind speed U_{10}. This example is for a pressure sensor with a noise floor $W = 2\times10^{-5}$ m^2 Hz^{-1} and a water column of 3 m depth. The wind speed is indicated by the contours of interval 4 m s^{-1}.

neglecting the Doppler-shift effect of the current led to larger errors in the estimation of mean wave period for all instruments.

Designing a field experiment —Using the criteria developed to define the optimal cutoff frequency, a relationship that assesses the ability of a pressure sensor to measure the smallest wave of interest at the depth of instrument deployment was developed. Combining Eq. 5 with the Case 2 criterion, found to optimally estimate wave heights from pressure data, the following expression can be developed

$$\frac{S_{\eta\eta}\left(1.1f_{pr}\right)K_p^2}{W} \geq 12\,, \qquad (13)$$

where W is the wide-band noise floor of the pressure sensor, f_{pr} is the relative peak frequency, and $S_{\eta\eta}$ is the surface wave spectra of interest. When the left side of Eq. 13 is greater than 12, the waves can be measured by the pressure sensor at the specified depth. If the noise floor of the instrument is unknown, then the instrument resolution specifications can be used to approximate the single estimate uncertainty R and the noise floor can be calculated via Eq. 12.

Prior to an experiment, the distribution of $S_{\eta\eta}$ will likely be unknown at the site of interest. In this case a model for $S_{\eta\eta}$ can be used to approximate $S_{\eta\eta}$ $(1.1f_{pr})$ for use in Eq. 13. The JONSWAP spectral form

$$S_{\eta\eta} = \alpha g^2 f^{-5}(2\pi)^{-4}\exp\left[-\frac{5}{4}\left(\frac{f}{f_{pr}}\right)^{-4}\right]\gamma^{\exp\left[\frac{(f-f_{pr})^2}{2\sigma^2 f_{pr}^2}\right]} \qquad (14)$$

has been found to effectively describe the spectrum of developing waves (e.g., Babanin and Soloviev 1998). Various researchers have used laboratory and field data sets to define the parameters in Eq. 14 as functions of environmental conditions such as fetch and wind speed. The parameters determined by Babanin and Soloviev (1998) are a reasonable choice for the underdeveloped waves present in enclosed or semi-enclosed water bodies, as their data set included underdeveloped waves. The various parameters in Eq. 14 are expressed as (Babanin and Soloviev 1998)

$$\begin{aligned}
\tilde{f}_{pr} &= \frac{U_{10}f_{pr}}{g} \\
\sigma &= 0.07 && \text{for } f \leq f_{pr} \\
&= 0.09 && \text{for } f > f_{pr} \\
\alpha &= 8.03\text{x}10^{-2}\,\tilde{f}_{pr}^{1.24} && \text{for } \tilde{f}_{pr} \leq 0.23 \\
&= 13.2\text{x}10^{-3} && \text{for } \tilde{f}_{pr} > 0.23 \\
\gamma &= 7.6\,\tilde{f}_{pr}
\end{aligned} \qquad (15)$$

where U_{10} is the wind speed 10 m above the water.

To illustrate the use of Eq. 13, we will assume we have an instrument with noise floor $W = 2 \times 10^{-5}$ m^2 Hz^{-1} and determine the maximum depth below the water surface at which the pressure sensor can be placed as a function of significant wave height, H_s, and peak frequency, f_{pr}, in a 3 m water column (Fig. 9). The wave spectra were calculated from specified f_{pr} and U_{10} via Eqs. 14 and 15, and the resultant H_s was calculated via Eq. 8. Results are shown for wind velocities ranging from 2 m s^{-1} to 20 m s^{-1}. For the same peak frequency the wave height increases as the wind velocity increases, therefore the maximum placement depth of the pressure sensor is larger. Figure 9 illustrates that placing the instrument on the bed severely restricts the waves measurable; the minimum H_s

measurable is approximately 0.3 m with maximum f_{pr} approximately 0.5 Hz.

The minimum wave measurable will also be a function of the mean water velocity, as the (intrinsic) spectral peak is shifted toward Nyquist frequency in a following current. Therefore, the second condition that must be met to enable the measurement of wind waves with pressure sensors is that the instrument can sample at least two times faster than the maximum f_i of interest

$$f_s \geq 2\left(1.1 f_{pr} + \frac{k\bar{u}\cos\theta}{2\pi}\right). \quad (16)$$

Comments and recommendations

The standard piezoelectric pressure sensors on a commercially available current meter were used to accurately measure wave heights of locally generated, short period ($T_{peak} < 2$ s) waves using the linear wave theory transformation. Including the Doppler-shift effect of the mean current reduced the error in the estimates of wave height and wave period. Due to the high frequency of the wind waves, a significant amount of wave energy existed at frequencies that were contaminated by noise. Therefore, identifying the best method for selecting the cutoff frequency and the implementation of a model for the equilibrium range of the wave spectrum was essential to gain an accurate estimate of the wave height.

The results from this study indicate that an effective method for deriving the wave spectrum from subsurface pressure measurements of high frequency waves is as follows:

1. Calculate the wave direction either from the measured directional wave spectra, without correcting for the Doppler effect of the mean current, or, to an approximation, from the measured wind direction.
2. Calculate the component of the equivalent unidirectional current in the direction of the waves.
3. Correct pressure data for changes in atmospheric pressure to accurately determine the pressure sensor depth. To calculate the pressure spectra S_{pp}, first divide each burst into segments of equal length, each with 50% overlap. Apply a Hanning window to each of the segments and ensemble average the fast Fourier transform of each segment to produce the spectral estimate (Bendat and Piersol 2000). Locate the noise floor of the instrument by averaging the flat portion of the spectrum in the high frequency range. Define the cutoff frequency such that the spectrum at that frequency is 12 times larger than the noise floor and greater than $1.1f_{peak}$. Apply linear wave theory to determine the transfer function, K_p, with correction of the dispersion relation for the Doppler effect due to the mean current (Eqs. 2, 3, and 4). Transform the pressure spectra, S_{pp}, into the (estimated) surface elevation spectra, $S^*_{\eta\eta}$ (Eq. 5).
4. Apply a f^{-4} tail beyond the cutoff frequency. Wave parameters can then be calculated from the estimated wave spectra (Eqs. 6 to 9).

Using this method the pressure sensors on the ADVs used in this study measured rms wave heights with an average error of 0.035 m and mean wave periods with an error of 0.13 s (errors at 95% confidence level). The results from this study illustrate that high-quality estimates of small, high-frequency waves in environments with significant unidirectional currents can be made with standard pressure sensors on commercially available current meters.

References

Anctil, F., and T. T. Quach. 1997. Control and analysis of manometric measurements on surface waves. Can. J. Civil Eng. 24:539-546.

Babanin, A. V., and Y. P. Soloviev. 1998. Field investigation of transformation of the wind wave frequency spectrum with fetch and the stage of development. J. Phys. Oceanogr. 28: 563-576.

Bendat, J., and A. Piersol. 2000. Random data: analysis and measurement procedures, 3rd ed. Wiley.

Bishop, C. T., and M. A. Donelan. 1987. Measuring waves with pressure transducers. Coast. Eng. 11:309-328.

Bricker, J. D., S. Inagaki, and S. G. Monismith. 2005. Bed drag coefficient variability under wind waves in a tidal estuary. J. Hydraul. Eng.-ASCE 131:497-508.

Cavaleri, L. 1980. Wave measurement using pressure transducer. Oceanolog. Acta 3:339-346.

Emery, W., and R. Thomson. 2001. Data analysis methods in physical oceanography. Elsevier.

Gabriel, D. W., and T. S. Hedges. 1986. Effects of currents on interpretation of subsurface pressure spectra. Coast. Eng. 10: 309-323.

Hashimoto, N., S. W. Thurston, and M. Mitsui. 1997. Surface wave recovery from subsurface pressure records on the basis of weakly nonlinear directional wave theory, p. 869-882. *In* B. L. E. a. M. Hemsley [ed.], Ocean wave measurement and analysis. Proceedings of the Third International Symposium Waves 97 held in Virginia Beach, Virginia, November 3–7, 1997, American Society of Civil Engineers Publications.

Hedges, T. S., and B. W. Lee. 1992. The equivalent uniform current in wave-current computations. Coast. Eng. 16:301-311.

Huntley, D. A., and D. G. Hazen. 1988. Seabed stresses in combined wave and steady flow conditions on the Nova-Scotia continental shelf: Field measurements and predictions. J. Phys. Oceanogr. 18:347-362.

Isobe, M., K. Kondo, and K. Horikawa. 1984. Extension of MLM for estimating directional wave spectrum, paper no. A-6. *In* Symposium on Description and Modelling of Directional Seas, June 1984, Technical University of Denmark.

Jones, N.L., and S. Monismith. 2007. Modeling the influence of wave enhanced turbulence in a shallow tide- and wind-driven water column. J. Geophys. Res. [doi: 10.1029/2007JC004246].

Johnson, D. 2002. DIWASP version 1.1, a directional wave spectra toolbox for MATLAB®: User manual. Centre for Water Research, University of Western Australia.

Kinsman, B. 1965. Wind waves: Their generation and propagation on the ocean surface. Prentice-Hall.

Kitaigorodskii, S. A. 1983. On the theory of the equilibrium range in the spectrum of wind-generated gravity-waves. J. Phys. Oceanogr. 13:816-827.

Kuo, Y. Y., and Y. F. Chiu. 1994. Transfer-function between wave height and wave pressure for progressive waves. Coast. Eng. 23:81-93.

Lee, D. Y., and H. Wang. 1984. Measurement of surface waves from subsurface gage, p. 271-286. *In* B. L. Edge [ed.], Nineteenth coastal engineering conference. Coastal Engineering.

Lowe, R. J., J. L. Falter, M. D. Bandet, G. Pawlak, M. J. Atkinson, S. G. Monismith, and J. R. Koseff. 2005. Spectral wave dissipation over a barrier reef. J. Geophys. Res.- Oceans 110 [doi:10.1029/2004JC002711].

May, C., J. Koseff, L. Lucas, J. Cloern, and D. Schoellhamer. 2003. Effects of spatial and temporal variability of turbidity on phytoplankton blooms. Mar. Ecol. Prog. Ser. 254:111-128.

Miller, H. C., and C. L. Vincent. 1990. FRF spectrum - TMA with Kitaigorodskii f^4 scaling. J. Waterway Port Coast. Ocean Eng.-ASCE 116:57-78.

Nortek AS. 2005. Vector current meter: User manual. Nortek AS.

Phillips, O. M. 1958. The equilibrium range in the spectrum of wind-generated waves. J. Fluid Mech. 4:426-433.

RBR. 2004. Wave height gauge, model wg-50: Owner's manual. RBR Ltd.

Smith, J. M. 2002. Wave pressure gauge analysis with current. J. Waterway Port Coast. Ocean Eng. ASCE 128:271-275.

Smith, M. J., C. L. Stevens, R. M. Gorman, J. A. McGregor, and C. G. Neilson. 2001. Wind-wave development across a large shallow intertidal estuary: A case study of Manukau Harbour, New Zealand. N. Z. J. Mar. Freshw. Res. 35:985-1000.

Stevens, C. L., and M. J. Smith. 2004. Temperature microstructure beneath surface gravity waves. J. Atmos. Ocean. Tech. 21:1747-1757.

Terray, E. A., M. A. Donelan, Y. C. Agrawal, W. M. Drennan, K. K. Kahma, A. J. Williams, P. A. Hwang, and S. A. Kitaigorodskii. 1996. Estimates of kinetic energy dissipation under breaking waves. J. Phys. Oceanogr. 26:792-807.

Trowbridge, J., and S. Elgar. 2001. Turbulence measurements in the surf zone. J. Phys. Oceanogr. 31:2403-2417.

Tsai, C.-H., F.-J. Young, M.-C. Huang, Y.-C. Lin, and H.-W. Li. 2001. Comparison of methods for recovering surface waves from pressure transducers p. 347-356. *In* B. L. Edge and J. M. Hemsley [eds.], Ocean wave measurement and analysis. ASCE.

———, M. C. Huang, F. J. Young, Y. C. Lin, and H. W. Li. 2005. On the recovery of surface wave by pressure transfer function. Ocean Eng. 32:1247-1259.

Tucker, M. J., and E. G. Pitt. 2001. Waves in ocean engineering. Elsevier.

Wang, H., D. Y. Lee, and A. Garcia. 1986. Time-series surface-wave recovery from pressure gauge. Coast. Eng. 10:379-393.

Wolf, J. 1997. The analysis of bottom pressure and current data for waves, p. 165-169. *In* 7th international conference on electronic engineering in oceanography, 23–25 June, 1997, Conference Publication No. 439, Institute of Electronic Engineers (IEE).

Zaslavskii, M. M., and V. P. Krasitskii. 2001. On the conversion of wave-gauge pressure data to the spectrum of surface waves. Oceanology 41:184-188.

Submitted 1 August 2006
Revised 4 July 2007
Accepted 5 July 2007